

# Coupled micro-resonators for second-order integrated nonlinear optics

Yannick Dumeige\*

*Université de Rennes, ENSSAT, CNRS, Institut FOTON-UMR 6082, 6 rue de Kerampont, 22300 Lannion, France*

Yoan Léger

*Université de Rennes, INSA Rennes, CNRS, Institut FOTON-UMR 6082, F-35000 Rennes, France*

(Dated: October 3, 2025)

We investigate second-order nonlinear processes in a system of two coupled identical optical micro-resonators. The double resonance and phase-matching conditions are simultaneously obtained thanks to the frequency splitting induced by the resonator coupling. The analysis made in the framework of the coupled mode theory is applied to the second harmonic generation process in two whispering gallery mode microdisks made in III-V materials.

Optical micro-resonators are of great interest for nonlinear photonics since they enable simultaneously, high integration, low power operation and high stability [1]. One of the most striking applications based on third order nonlinear optics in micro-resonators is the integration of frequency comb sources on a chip [2]. second-order nonlinear optics can also take benefit from the use of optical micro-resonators which could lead to the miniaturization of frequency converters, optical parametric oscillators or entangled photon sources [3]. In this aim, the platform of III-V semiconductors is promising since they have high second-order susceptibilities, high refractive index and direct band gap which let envisage micro- or nano-photonics nonlinear or quantum active devices [4] in a wide spectral band. Considering GaP for instance, the transparency domain ranges from  $0.55 \mu\text{m}$  to  $11 \mu\text{m}$  [5] up to wavelength inaccessible to lithium niobate. III-V materials are isotropic, thus birefringence phase matching is not possible and several methods have been demonstrated to circumvent this issue [6–10]. In this context, natural quasi-phase matching in semiconductor whispering gallery mode (WGM) resonators have been proposed [11, 12] and experimentally demonstrated [13]. Nevertheless, due to the very high dispersion of III-V semiconductors, practical implementations of this quasi-phase matching scheme also rely on the use of modal phase matching [14–16] reducing the effective nonlinear susceptibility due to a low interacting fields overlap. Furthermore, complex numerical techniques can be implemented to optimize the phase matching and the nonlinear overlap in the design of doubly resonant nonlinear photonic structures [17–19]. From another point of view, it has been shown that the coupling of several resonators or of counter-propagating modes within a single resonator allows the control or the engineering of the dispersion in  $\chi^{(3)}$  processes [20–22]. Coupled resonator structures can be used to reach functionalities which are not attainable with single nonlinear resonators [23]. If we restrict ourselves to the case of second-order effects, only few works have been devoted to the coupling of nonlinear micro-

resonators [24–26]. In particular, it has been shown in the tight binding approximation that the dispersion induced by the weak coupling of resonators can be used to reach the phase matching condition for SHG in a long chain of  $\chi^{(2)}$  microcavities [24].

In this paper, we propose a simple and comprehensive design method using the unique properties of the coupling between two identical WGM resonators to obtain the phase matching condition. Using a benchmark of GaP WGM microdisks, we show that the strong coupling between two resonators helps to reach the natural quasi-phase matching condition with low radial order modes in the process of second harmonic generation (SHG). This approach would lead to reach the low-power high-conversion regime on a chip.

Figure 1 is a sketch of the structure studied in this paper. It consists of two rings or disks of radius  $R = L/\pi$  mutually coupled due to the overlap of the evanescent part of their modes. The resonators are coupled to two insertion and extraction waveguides with the same rate. The curvilinear abscissa along the resonator is called  $s$ . The fundamental (F) fields are denoted  $A_i(s) = \mathcal{A}_i(s)e^{j(\omega t - \beta_1 s)}$  and the second harmonic (SH) fields  $B_i(s) = \mathcal{B}_i(s)e^{j(2\omega t - \beta_2 s)}$  with  $i \in [1, 8]_{\mathbb{N}}$  and where  $\beta_1(\omega)$  and  $\beta_2(2\omega)$  are respectively the propagation constants of the F and SF modes whose angular frequencies are respectively  $\omega$  and  $2\omega$ .  $k_i$  and  $t_i$  are the coupling and transmission coefficients (with  $|k_i|^2 + |t_i|^2 = 1$ ) between the guides and the resonators, we can write the corresponding coupling matrices [27]

$$M_i = \begin{pmatrix} t_i & k_i \\ -k_i^* & t_i^* \end{pmatrix} \quad (1)$$

where  $i = 1$  for the F field and  $i = 2$  for the SH field. The coupling between the two resonators is described by two coefficients  $\kappa_i$  and  $\tau_i$  (with also  $|\kappa_i|^2 + |\tau_i|^2 = 1$ ) and thus by the matrix

$$P_i = \begin{pmatrix} \tau_i & \kappa_i \\ -\kappa_i^* & \tau_i^* \end{pmatrix}. \quad (2)$$

We have for instance  $(A_T \ A_1)^T = M_1(A_{in} \ A_4)^T$ ,  $(B_D \ B_7)^T = M_2(0 \ B_6)^T$  and  $(A_3 \ A_5)^T = P_1(A_2 \ A_8)^T$ .

\* yannick.dumeige@univ-rennes.fr

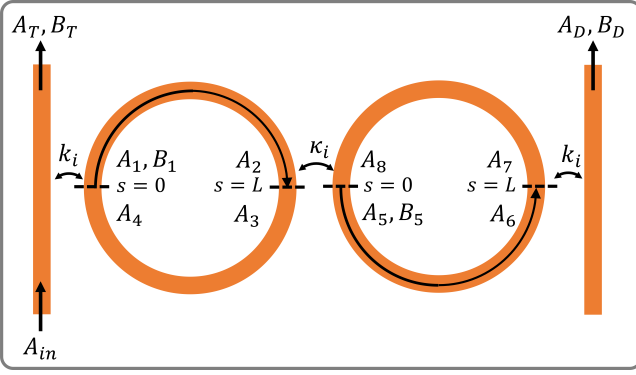


FIG. 1. System of coupled ring or disk resonators of perimeter  $2L$ .  $A_i$  and  $B_i$  are the F and SH mode amplitudes within the structure.  $k_i$  are the coupling between the access bus waveguides and the structure.  $\kappa_i$  are the coupling coefficient between the two resonators.  $A_{in}$  is the input F mode amplitude.  $A_T$  and  $B_T$  are the F and SH output mode amplitude on the trough port.  $A_D$  and  $B_D$  are the output mode amplitude on the drop port.

We consider that the pump is undepleted and thus all the calculations are linear for the F fields. Using the matrices  $M_1$  and  $P_1$  it is straightforward to calculate the field  $A_i(s)$  at each point of the system [23]. In the case of zinc-blende symmetry materials such as GaP, the second-order nonlinear susceptibility depends on  $s$  in the form  $\chi^{(2)}(s) = \chi_{0+}^{(2)} e^{j\frac{2s}{R}} + \chi_{0-}^{(2)} e^{-j\frac{2s}{R}}$  [11, 28]. The SH field is then calculated along each half perimeter of the resonator by integrating the following equation

$$\frac{dB_{2p+1}}{ds} = A_{2p+1}^2(s_0) \left( \chi_{0+}^{(2)} e^{j\frac{2s}{R}} + \chi_{0-}^{(2)} e^{-j\frac{2s}{R}} \right) e^{j\Delta\beta s} \quad (3)$$

for  $p \in [0, 3]_{\mathbb{N}}$  with  $\Delta\beta = \beta_2 - 2\beta_1$ ;  $s_0 = 0$  for  $p = \{0, 2\}$  and  $s_0 = L$  for  $p = \{1, 3\}$ . Defining  $\varphi_2 = -\beta_2 L$ , we obtain the expression of the amplitude of the output field on the trough port

$$B_T = k_2 K e^{j\varphi_2} \frac{[H_2 A_1^2 + \frac{\kappa_2}{D} (t_2^* A_5^2 + A_7^2 e^{-j\varphi_2}) + A_3^2 e^{-j\varphi_2}]}{1 - t_2^* H_2 e^{2j\varphi_2}} \quad (4)$$

with

$$D = 1 - t_2^* \tau_2^* e^{2j\varphi_2}, \quad (5)$$

and where  $H_2(2\omega)$  is the linear transfer function of the right microdisk for the SH field (see Fig. 1)

$$H_2 = \frac{\tau_2 - t_2^* e^{2j\varphi_2}}{1 - t_2^* \tau_2^* e^{2j\varphi_2}}. \quad (6)$$

For zinc-blende symmetry materials, the nonlinear coupling is characterized by

$$K = j \left[ \chi_{0+}^{(2)} \frac{1 - e^{j\widetilde{\Delta\beta}_+ L}}{\widetilde{\Delta\beta}_+} + \chi_{0-}^{(2)} \frac{1 - e^{-j\widetilde{\Delta\beta}_- L}}{\widetilde{\Delta\beta}_-} \right] \quad (7)$$

where the effective phase mismatch  $\widetilde{\Delta\beta}_{\pm}$  is defined as

$$\widetilde{\Delta\beta}_{\pm} = \Delta\beta \pm \frac{2}{R}. \quad (8)$$

In standard nonlinear photonic devices, the effective index mismatch between the F and SH modes depends only on the material and modal dispersions. It is independent of the cavity length (or micro-resonator radius). On the contrary, the phase mismatch compensation offered by the  $\bar{4} \chi^{(2)}$  tensor symmetry, see (Eq. 8), as well as the maximal splitting of coupled resonators both scale with the free spectral range (FSR). Their cumulated effect thus requires small geometries to effectively cancel the effective index mismatch. We apply the previous model to the case of two identical coupled GaP microdisks grown along the  $z = [001]$  crystallographic axis and embedded in air as described in Fig. 2. The disks are separated by an air gap  $g$ , their thickness is  $H = 136$  nm and their radius  $R = 2.7 \mu\text{m}$ . The properties of the system is ob-

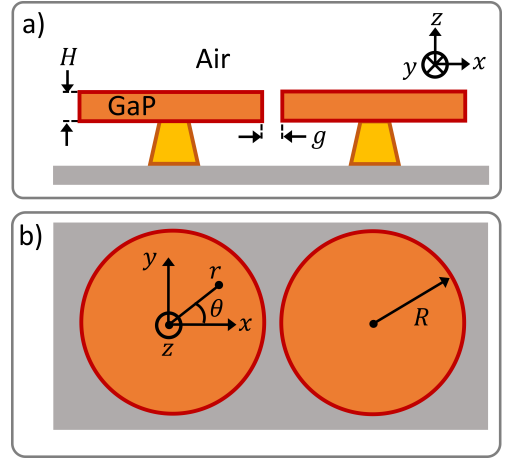


FIG. 2. Description of the structure numerically studied consisting of two GaP WGM microdisks embedded in air. a) side view and b) top view.  $g$  is the air gap separating the two disks,  $H$  and  $R$  are their thickness and radius.

tained from the optical properties of a single resonator. The confinement in the  $z$ -direction is taken into account using the effective index method (EIM) [29]. We used the lowest order guided modes in the  $z$ -direction both for the F and SH frequencies to optimize the effective nonlinear susceptibility. Due to the  $\bar{4}3m$  symmetry of the GaP, the F field is chosen polarized in the  $(x, y)$  plan which gives an SH field polarized in the  $z$ -direction. Thus in the EIM framework, the F field is TE polarized whereas the SH field in TM polarized. The effective propagation constants calculated using this approximation are noted  $\gamma_1$  and  $\gamma_2$  respectively for the F and SF fields. The propagation constants  $\beta_1$  and  $\beta_2$  of the two modes are obtained solving the Helmholtz equation for a cylinder of refractive index  $\gamma_{1,2}/k_0$  (with  $k_0(\omega)$  the free space wavevector) surrounded by air. Note that for both frequencies we have chosen the modes with the lowest radial order to

reach a good overlap of the interacting fields and thus a maximal effective non-linear susceptibility [11]. In this case it is not possible to use the modal phase matching technique to compensate for the dispersion to reach the phase matching condition. Figure 3.a) shows the linear transmission spectra for a single disk on the drop port assuming that the intrinsic and coupling quality (Q) factors are equal to  $10^4$ .  $\nu_F$  is the F mode frequency, the frequency  $\nu_{SH}$  of the SH field has been divided by two for the sake of clarity. Due to the strong material and

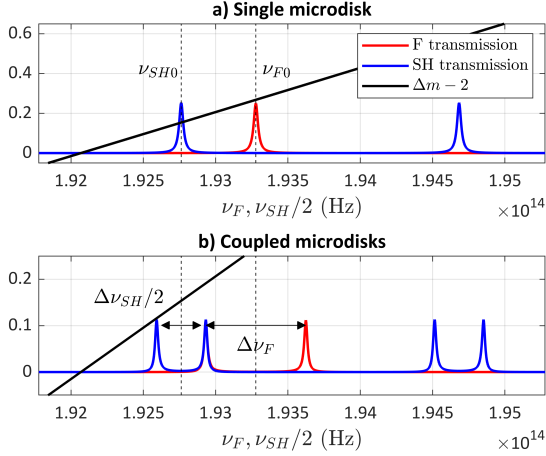


FIG. 3. Transmission spectra calculated on the drop port and azimuthal quantum number mismatch. a) for a single resonator the double resonance  $\nu_{F0} = \nu_{SH0}/2$  and the condition  $|\Delta m - 2| < 1/2$  can not be fulfilled due to the dispersion. b) By coupling the two disks it is possible to reach both conditions simultaneously.

form dispersions it is not possible to reach the double resonance with a difference in the phase mismatch such as  $\Delta m - 2 = 0$  (where  $\Delta m = \Delta\beta R$  is the phase mismatch in term of azimuthal quantum numbers), consequently  $\nu_{F0}$  and  $\nu_{SH0}$  the resonant frequencies for the F and the SH modes giving a minimal phase mismatch do not coincide and  $\nu_{F0} > \nu_{SH0}/2$ . The double resonance  $\nu_{F0} = \nu_{SH0}/2$  could be obtain but with  $\Delta m - 2$  equal to an integer strictly positive which would lead to a null SHG over a circumference of the resonator. By coupling two identical resonators, the F and SH resonances are split by respectively  $\Delta\nu_F$  and  $\Delta\nu_{SH}$ , values depending on  $g$ . If we define the new frequency mismatch between the split resonant frequencies

$$\delta(g) = \frac{\nu_{SH0}}{2} - \nu_{F0} - \frac{1}{2} \left( \Delta\nu_F(g) + \frac{\Delta\nu_{SH}(g)}{2} \right) \quad (9)$$

it is possible to find an air-gap value  $g_0$  which makes the two inner F and SH frequencies to match reaching the phase matching as shown in Fig. 3.b). At the same time we have  $|\Delta m - 2| < 1/2$  which insures an efficient SHG over the perimeter of each resonator. To find the value of  $g_0$  we used a home-made FDTD code [30] to calculate

the linear spectra around F and SH frequencies for the coupled structure for several values of  $g$ . Thus, the de-

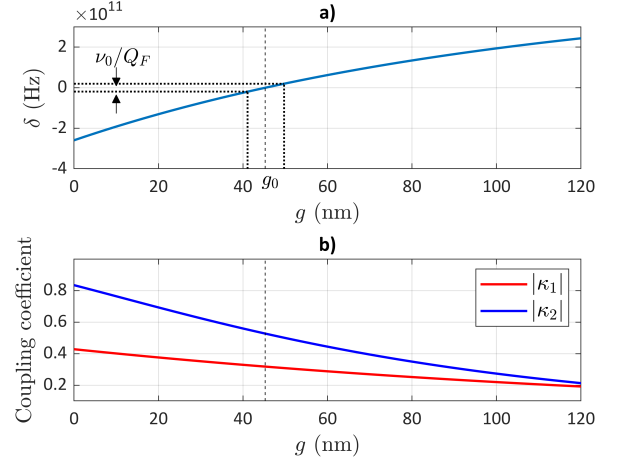


FIG. 4. a) Nonlinear detuning  $\delta(g)$  calculated using a combinations of FDTD simulations and EIM. b) Coupling coefficients  $\kappa_1$  and  $\kappa_2$  deduced from FDTD simulations. The vertical dashed line gives the air gap value  $g_0$  fulfilling the double resonance condition.

tuning  $\delta$  can be calculated varying the air-gap as shown in Fig. 4.a). Note that to produce the results given Fig. 4, we interpolated the numerical discrete calculations of  $\Delta\nu_F(g)$  and  $\Delta\nu_{SH}(g)$  using decaying exponential functions. The corresponding coupling coefficients necessary to calculate the SHG in the coupled mode framework using Eq. (4) are deduced from  $|\kappa_1| = \sin\left(\frac{\pi\Delta\nu_F}{\Delta_1}\right)$  and  $|\kappa_2| = \sin\left(\frac{\pi\Delta\nu_{SH}}{\Delta_2}\right)$  where  $\Delta_1$  and  $\Delta_2$  are respectively the FSR for the F and SH fields [31], the resulting values are plotted in Fig. 4.b). For a microdisk, the effective nonlinear susceptibilities is calculated for the single resonator WGM modes of resonant frequencies  $\nu_{F0}$  and  $\nu_{SH0}$  and azimuthal quantum numbers  $m_1 = 17$  and  $m_2 = 36$ . Cylindrical coordinates  $(r, \theta)$  are defined in Fig. 2 and  $d_{14} = 28.5$  pm/V is the nonlinear coefficient of bulk GaP [32]. From the coupling mode theory [11] we find

$$\chi_{0\pm}^{(2)} = -\frac{j\gamma_2}{4R^2N_2^2} \int_0^R r^2 d_{14} f_{\pm}(r) (\mathcal{H}_r^{SH})^* dr, \quad (10)$$

where  $N_2$  is the bulk refractive index of GaP at the SH frequency. In expression (10) we have assumed that

$$f_{\pm}(r) = \mathcal{E}_r^F \mathcal{E}_\theta^F \pm j \frac{(\mathcal{E}_r^F)^2 - (\mathcal{E}_\theta^F)^2}{2}. \quad (11)$$

The F electric fields can be expressed using  $J_\alpha$  the first kind Bessel functions of order  $\alpha$

$$\mathcal{E}_r^F = -\frac{am_1}{r\epsilon_0} \left( \frac{2\pi\nu_{F0}}{\gamma_1 c} \right)^2 J_{m_1}(\gamma_1 r) \quad (12)$$

and

$$\mathcal{E}_\theta^F = -\frac{j}{m_1} \frac{d(r\mathcal{E}_r^F)}{dr}. \quad (13)$$

Eventually, the SH magnetic field is given by

$$\mathcal{H}_r^{SH}(r) = bJ_{m_2}(\gamma_2 r). \quad (14)$$

The constants  $a$  and  $b$  are calculated in order that  $|\mathcal{A}_i|^2$  and  $|\mathcal{B}_i|^2$  correspond to the power flows for the F and SH modes in W/m [11]. Figure 5 represents the normalized

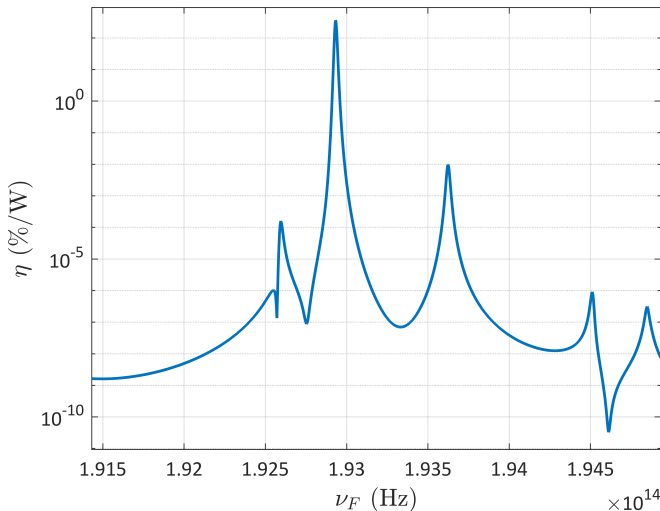


FIG. 5. Conversion efficiency  $\eta(\nu_F)$  calculated for  $\delta(g_0) = 0$ .

conversion efficiency  $\eta = \frac{|B_T|^2}{|A_{in}|^2 \mathcal{P}_{in}}$  (where  $\mathcal{P}_{in}$  is the input F power) for the studied structure in the case  $g = g_0$ . For the doubly resonant frequency we obtain a maximal conversion efficiency of 360%/W which is consistent with results calculated for small thin microdisks (with same Q-factors) under perfect phase matching [32]. This result shows that even though we obtained the double resonance with two supermodes with different symmetry it does not affect the efficiency of the device. The interest of the proposed method is that the resonator coupling gives an additional free parameter which would allow to use

thicker and largest disks which would be less sensitive to fabrication imperfections. As with single doubly resonant resonators, the disk radius must be controlled with an accuracy of the order of  $R/Q_F$ . In the example presented, this gives 0.5 nm. For practical implementation, it will be necessary to control the resonances independently, using, for example, thermal effects [33]. Another solution could be to use a single corrugated disk and take advantage of the coupling of co- and counter-propagating modes [34]. This would mean that only one resonator would need to be controlled. If we suppose a tolerance of  $\nu_{F0}/Q_F$  (with  $Q_F$  the loaded Q-factor for the F) for the double resonance in frequency it translates in a 10 nm fabrication tolerance for the air-gap. Note that the relative phase between the two coupling coefficients  $\kappa_1$  and  $\kappa_2$  has a negligible effect on the conversion efficiency maximum.

We have proposed a new method to reach the phase matching condition in second-order nonlinear processes in integrated optics relying on the use of the frequency splitting due to the coupling of identical resonators. We show how this phase matching scenario could be implemented using GaP microdisks to reach conversion yields such high as 360%/W with micron-size devices. The resonator coupling could also be used as the additional free parameter required to reach the double resonance condition in single mode nonlinear Fabry-Perot microcavities [35]. This method could be straightforwardly applied to a chain of three resonators which could be useful to reach higher frequency splittings for a given coupling strength between resonators enabling the compensation of larger phase-mismatch. Finally our approach could be profitably applied to the SHG in nano-resonators [36] such as coupled photonic crystal cavities. Indeed, since the splitting strongly depends on the FSR of the cavity, huge detuning as high as several nanometers could be canceled in these ultimately short cavities [37].

## FUNDING INFORMATION

This research was supported by the French National Research Agency (ANR) through the JCJC Orpheus project (ANR-17-CE24-0019) and the "France 2030" OF-COC project (ANR-22-PEEL-0005).

- 
- [1] G. Lin, A. Coillet, and Y. K. Chembo, "Nonlinear photonics with high-Q whispering-gallery-mode resonators," *Adv. Opt. Photon.* **9**, 828–890 (2017).
  - [2] B. Stern, X. Ji, Y. Okawachi, A. L. Gaeta, and M. Lipson, "Battery-operated integrated frequency comb generator," *Nature* **562**, 401 (2018).
  - [3] P. Liu, H. Wen, L. Shi, and X. Zhang, " $\chi^{(2)}$  nonlinear photonics in integrated microresonators," *Frontiers of Optoelectronics* **16**, 18 (2023).
  - [4] F. Baboux, G. Moody, and S. Ducci, "Nonlinear integrated quantum photonics with AlGaAs," *Optica* **10**, 917–931 (2023).
  - [5] Y. Wang, Z. Pan, Y. Yan, Y. Yang, W. Zhao, N. Ding, X. Tang, P. Wu, Q. Zhao, and Y. Li, "A review of gallium phosphide nanophotonics towards omnipotent nonlinear devices," *Nanophotonics* **13**, 3207–3252 (2024).
  - [6] A. Fiore, S. Janz, L. Delobel, P. van der Meer, P. Bravetti, V. Berger, E. Rosencher, and J. Nagle, "Second-harmonic generation at  $\lambda=1.6 \mu\text{m}$  in AlGaAs/Al<sub>2</sub>O<sub>3</sub> waveguides using birefringence phase matching," *Applied Physics Letters* **72**, 2942–2944 (1998).

- [7] Y. Dumeige, I. Sagnes, P. Monnier, P. Vidakovic, I. Abram, C. Mériadec, and A. Levenson, “Phase-matched frequency doubling at photonic band edges: Efficiency scaling as the fifth power of the length,” *Phys. Rev. Lett.* **89**, 043901 (2002).
- [8] S. Ducci, L. Lanco, V. Berger, A. De Rossi, V. Ortiz, and M. Calligaro, “Continuous-wave second-harmonic generation in modal phase matched semiconductor waveguides,” *Applied Physics Letters* **84**, 2974–2976 (2004).
- [9] A. S. Helmy, “Phase matching using bragg reflection waveguides for monolithic nonlinear optics applications,” *Opt. Express* **14**, 1243–1252 (2006).
- [10] K. Pantzas, S. Combré, M. Bailly, R. Mandouze, F. R. Talenti, A. Harouri, B. Gérard, G. Beaudoin, L. Le Gratiet, G. Patriarche, A. De Rossi, Y. Léger, I. Sagnes, and A. Grisard, “Continuous-wave second-harmonic generation in orientation-patterned gallium phosphide waveguides at telecom wavelengths,” *ACS Photonics* **9**, 2032–2039 (2022).
- [11] Y. Dumeige and P. Féron, “Whispering-gallery-mode analysis of phase-matched doubly resonant second-harmonic generation,” *Phys. Rev. A* **74**, 063804 (2006).
- [12] A. Lorenzo-Ruiz and Y. Léger, “Generalization of second-order quasi-phase matching in whispering gallery mode resonators using berry phase,” *ACS Photonics* **7**, 1617–1621 (2020).
- [13] P. S. Kuo, J. Bravo-Abad, and G. S. Solomon, “Second-harmonic generation using quasi-phases matching in a GaAs whispering-gallery-mode microcavity,” *Nature Communications* **5**, 3109 (2014).
- [14] S. Mariani, A. Andronico, A. Lemaître, I. Favero, S. Ducci, and G. Leo, “Second-harmonic generation in AlGaAs microdisks in the telecom range,” *Opt. Lett.* **39**, 3062–3065 (2014).
- [15] D. P. Lake, M. Mitchell, H. Jayakumar, L. F. dos Santos, D. Curic, and P. E. Barclay, “Efficient telecom to visible wavelength conversion in doubly resonant gallium phosphide microdisks,” *Applied Physics Letters* **108**, 031109 (2016).
- [16] L. Chang, A. Boes, P. Pintus, J. D. Peters, M. Kennedy, X.-W. Guo, N. Volet, S.-P. Yu, S. B. Papp, and J. E. Bowers, “Strong frequency conversion in heterogeneously integrated GaAs resonators,” *APL Photonics* **4**, 036103 (2019).
- [17] C. Simonneau, J. P. Debray, J. C. Harmand, P. Vidaković, D. J. Lovering, and J. A. Levenson, “Second-harmonic generation in a doubly resonant semiconductor microcavity,” *Opt. Lett.* **22**, 1775–1777 (1997).
- [18] Z.-F. Bi, A. W. Rodriguez, H. Hashemi, D. Duchesne, M. Loncar, K.-M. Wang, and S. G. Johnson, “High-efficiency second-harmonic generation in doubly-resonant  $\chi^{(2)}$  microring resonators,” *Opt. Express* **20**, 7526–7543 (2012).
- [19] Z. Lin, X. Liang, M. Lončar, S. G. Johnson, and A. W. Rodriguez, “Cavity-enhanced second-harmonic generation via nonlinear-overlap optimization,” *Optica* **3**, 233–238 (2016).
- [20] A. Armaroli, P. Féron, and Y. Dumeige, “Stable integrated hyper-parametric oscillator based on coupled optical microcavities,” *Opt. Lett.* **40**, 5622–5625 (2015).
- [21] X. Lu, Y. Sun, A. Chanana, U. A. Javid, M. Davanco, and K. Srinivasan, “Multi-mode microcavity frequency engineering through a shifted grating in a photonic crystal ring,” *Photon. Res.* **11**, A72–A79 (2023).
- [22] S. Sanyal, Y. Okawachi, Y. Zhao, B. Y. Kim, K. J. McNulty, M. Lipson, and A. L. Gaeta, “Nonlinear dynamics of coupled-resonator kerr combs,” *Phys. Rev. Lett.* **134**, 123801 (2025).
- [23] Y. Dumeige, L. Ghisa, and P. Féron, “Integrated all-optical pulse restoration with coupled nonlinear microring resonators,” *Opt. Lett.* **31**, 2187–2189 (2006).
- [24] Y. Xu, R. K. Lee, and A. Yariv, “Propagation and second-harmonic generation of electromagnetic waves in a coupled-resonator optical waveguide,” *J. Opt. Soc. Am. B* **17**, 387–400 (2000).
- [25] Y. Dumeige, “Miniaturization of fresnel phase matching using a side-coupled integrated spaced sequence of resonators (scissor),” *Opt. Lett.* **32**, 3438–3440 (2007).
- [26] Y. Dumeige, “Quasi-phase-matching and second-harmonic generation enhancement in a semiconductor microresonator array using slow-light effects,” *Phys. Rev. A* **83**, 045802 (2011).
- [27] A. Yariv, “Universal relations for coupling of optical power between microresonators and dielectric waveguides,” *Electronics Letters* **36**, 321–322 (2000).
- [28] Z. Yang, P. Chak, A. D. Bristow, H. M. van Driel, R. Iyer, J. S. Aitchison, A. L. Smirl, and J. E. Sipe, “Enhanced second-harmonic generation in AlGaAs microring resonators,” *Opt. Lett.* **32**, 826–828 (2007).
- [29] P. S. Kuo and G. S. Solomon, “On- and off-resonance second-harmonic generation in GaAs microdisks,” *Opt. Express* **19**, 16898–16918 (2011).
- [30] N. Jebali, L. Bodiou, J. Charrier, A. Armaroli, and Y. Dumeige, “Combining ftd and coupled-mode theory for self-pulsing modeling in coupled nonlinear microring resonators,” *J. Opt. Soc. Am. B* **37**, 2557–2563 (2020).
- [31] D. D. Smith, H. Chang, and K. A. Fuller, “Whispering-gallery mode splitting in coupled microresonators,” *J. Opt. Soc. Am. B* **20**, 1967–1974 (2003).
- [32] P. Guillemé, M. Vallet, J. Stodolna, A. Ponchet, C. Cornet, A. Létoublon, P. Féron, O. Durand, Y. Léger, and Y. Dumeige, “Antiphase domain tailoring for combination of modal and  $\bar{4}$ -quasi-phase matching in gallium phosphide microdisks,” *Opt. Express* **24**, 14608–14617 (2016).
- [33] M. Borghi, A. Trenti, and L. Pavesi, “Four Wave Mixing control in a photonic molecule made by silicon microring resonators,” *Sci. Rep.* **9**, 408 (2019).
- [34] C. Shirpurkar, J. Zang, K. Y. Yang, D. Carlson, S. P. Yu, E. Lucas, S. V. Pericherla, J. Yang, M. Guidry, D. Lukin, G. H. Ahn, J. Lu, L. Trask, F. Aflatouni, J. Vučković, S. B. Papp, and P. J. Delfyett, “Photonic crystal resonators for inverse-designed multi-dimensional optical interconnects,” *Opt. Lett.* **47**, 3063 (2022).
- [35] V. Berger, “Second-harmonic generation in monolithic cavities,” *J. Opt. Soc. Am. B* **14**, 1351–1360 (1997).
- [36] F. Raineri, Y. Dumeige, A. Levenson, and X. Letartre, “Nonlinear decoupled ftd code: phase-matching in 2d defective photonic crystal,” *Electronics Letters* **38**, 1704–1706 (2002).
- [37] S. Azzini, D. Grassani, M. Galli, D. Gerace, M. Patrini, M. Liscidini, P. Velha, and D. Bajoni, “Stimulated and spontaneous four-wave mixing in silicon-on-insulator coupled photonic wire nano-cavities,” *Applied Physics Letters* **103**, 031117 (2013).

# Coupled micro-resonators for second-order integrated nonlinear optics: Supplemental document

## I. EFFECT OF A DEVIATION FROM THE NOMINAL RADIUS VALUE

In the calculations shown in the main paper, we considered that the two microdisks have the same radius  $R = R_0 = 2.7 \mu\text{m}$  leading to doubly resonant SHG for the F frequency  $\nu_0$ . In this section we assume also that the radius of the first microdisk (located on the left of the structure) has the nominal value  $R_1 = R_0$  but we consider that the second microdisk has a radius ( $R_2$ ) slightly deviating from the nominal value such as  $R_2 = R_0 + \Delta R$ . Figure S1 shows the

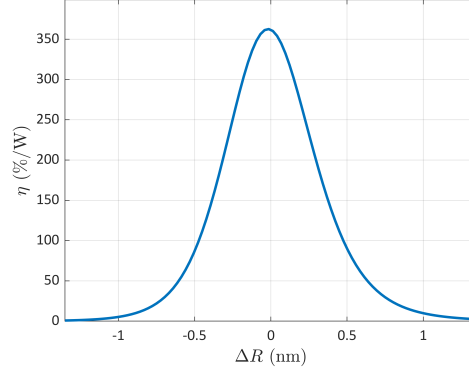


FIG. S1. Normalized conversion efficiency calculated for  $R_1 = R_0$  and  $R_2 = R_1 + \Delta R$ .

normalized conversion efficiency  $\eta$  as a function of  $\Delta R$ . The FWHM of the curve is 0.68 nm which is comparable to  $R/Q_F = 0.54 \text{ nm}$  where  $Q_F = 5 \times 10^3$  is the common value of the loaded Q-factors for the F and SH fields (for F and SH fields we considered intrinsic and coupling Q-factors of  $10^4$  leading to a loaded Q-factor of  $5 \times 10^3$ ).

## II. EFFECT OF THE RELATIVE PHASE BETWEEN THE COUPLING COEFFICIENTS $\kappa_1$ AND $\kappa_2$

In the main paper, we assume that the coupling coefficients between the two resonators  $\kappa_1$  and  $\kappa_2$  are imaginary numbers but from a general point of view these quantities are complex numbers [1]. The relative phase between these coefficients called  $\theta$  such as  $\kappa_2 = \kappa_1 e^{j\theta}$  is not easily obtained using the numerical method we used. Note that the phase

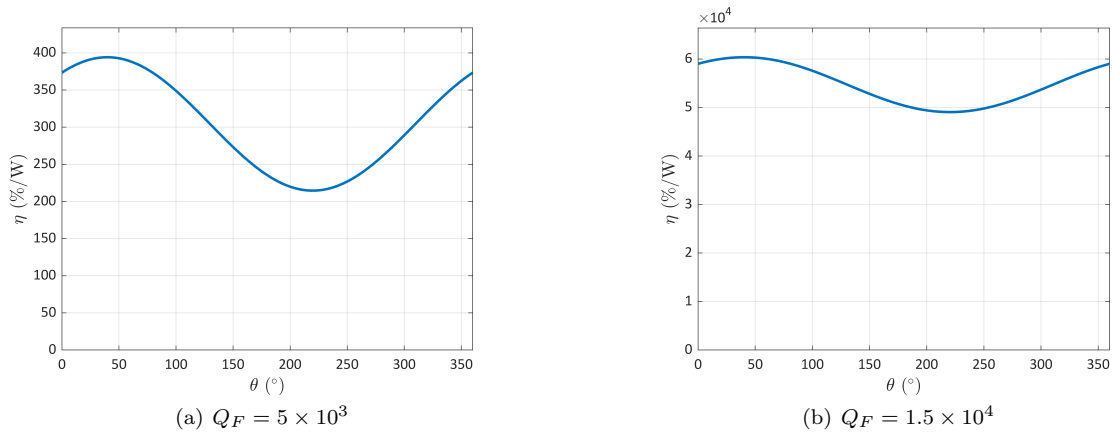


FIG. S2. Normalized conversion efficiency calculated for  $R_1 = R_2 = R_0$  and a varying phase  $\theta$  between the two coupling coefficients  $\kappa_1$  and  $\kappa_2$  and for equal loaded Q-factors at F and SH frequencies: (a)  $5 \times 10^3$  (b) for  $1.5 \times 10^4$ .

of the coupling coefficient gives the spectral position of the odd and even modes. This depends strongly on the precise geometry of the coupling area [2]. To go further, we calculate here in Fig. S2 the conversion efficiency as a function of  $\theta$  for two values of the intrinsic Q-factors. We can observe that in our case the relative phase between the two modes decreases the conversion efficiency only by a factor 2. If we increase the Q-factor this effects is reduced. Indeed by increasing the Q-factor, the second resonator acts as an all pass-filter in this case at the coupling point between the two resonators, the coupled SH field coming from the second resonator is much larger than the transmitted SH field reducing the detrimental effect of the interference between these two fields.

### III. INFLUENCE OF THE AIR GAP VALUE ON THE CONVERSION EFFICIENCY

In Fig. S3 we have calculated the variation of the conversion efficiency as a function of  $g$  for the structure described in the article. We can see that the FWHM of the curve is 5 nm which is comparable to the 10 nm found in the main article using a qualitative method.

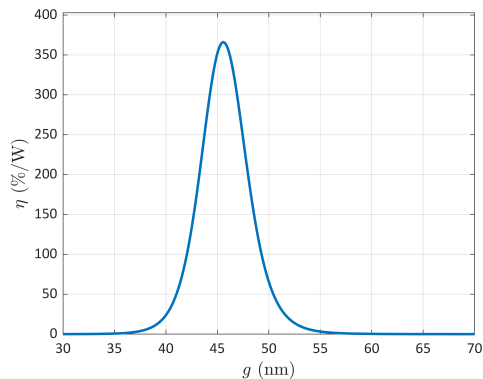


FIG. S3. Normalized conversion efficiency calculated for  $R_1 = R_2 = R_0$  and a varying air gap value  $g$ .

### IV. LIST OF THE PHYSICAL PARAMETERS

In Table I we give an exhaustive list of all the physical quantities and parameters used in the main article.

- 
- [1] A. Yariv, Universal relations for coupling of optical power between microresonators and dielectric waveguides, *Electronics Letters* **36**, 321 (2000).
  - [2] A. Perrier, Y. Guilloit, E. Le Cren, and Y. Dumeige, A simple model system to study coupled photonic crystal microcavities, *American Journal of Physics* **89**, 538 (2021).

TABLE I. Physical quantities and structural parameters.

$R$	Radius of the microdisks
$L$	Half perimeter of the microdisks: $L = \pi R$
$s$	Curvilinear abscissa: $s = R\theta$
$\omega$	Angular frequency
$A_i(s)$	Fundamental fields $i \in [1, 8]_{\mathbb{N}}$
$B_i(s)$	SH fields $i \in [1, 8]_{\mathbb{N}}$
$\mathcal{A}_i(s)$	F slowly varying field envelops $i \in [1, 8]_{\mathbb{N}}$
$\mathcal{B}_i(s)$	SH slowly varying field envelops $i \in [1, 8]_{\mathbb{N}}$
$k_i$	Coupling coefficients between the guide and the disks, $i = 1$ for the F and $i = 2$ for the SH
$\kappa_i$	Coupling coefficients between the two disks, $i = 1$ for the F and $i = 2$ for the SH
$M_i$	$2 \times 2$ coupling matrices waveguide/resonators, $i = 1$ for the F and $i = 2$ for the SH
$P_i$	$2 \times 2$ coupling matrices resonator/resonator, $i = 1$ for the F and $i = 2$ for the SH
$\beta_i$	Propagation constants of the resonant modes, $i = 1$ for the F and $i = 2$ for the SH
$\Delta\beta$	Propagation constant mismatch, $\Delta\beta = \beta_2 - 2\beta_1$
$\Delta m$	Normalized phase mismatch, $\Delta m = \Delta\beta R$
$\widetilde{\Delta\beta}_{\pm}$	Effective propagation constant mismatches, $\widetilde{\Delta\beta}_{\pm} = \Delta\beta \pm \frac{2}{R}$
$\varphi_2$	Accumulated phase over a perimeter at SH frequency, $\varphi_2 = -\beta_2 L$
$H$	Thickness of the microdisks
$g$	Air gap
$g_0$	Air gap value giving the double resonance
$\gamma_i$	Propagation constant of the vertically confined modes, $i = 1$ for the F and $i = 2$ for the SH
$k_0(\omega)$	Free space wavevector
$\nu_F$ and $\nu_{SH}$	Frequencies of the F and SH fields
$\nu_{F0}$ and $\nu_{SH0}$	Resonant frequencies of the F and SH fields of a single microdisk
$\Delta\nu_F$ and $\Delta\nu_{SH}$	Frequency splittings for the F and SH fields
$\Delta_i$	Free spectral ranges, $i = 1$ for the F and $i = 2$ for the SH
$N_2$	GaP bulk refractive index for the SH field
$d_{14}$	Nonlinear coefficient of GaP: $d_{14} = 28.5$ pm/V
$m_i$	Azimuthal quantum numbers of the resonant modes, $i = 1$ for the F and $i = 2$ for the SH
$\mathcal{P}_{in}$	Optical power of the incident F signal
$\eta$	Normalized conversion efficiency in %/W
$A_{in}$	Incident F field
$B_T$	Generated SH field propagating in the through port
$Q_F$	Loaded Q-factor at the F frequency